![WATCH Water and Global Change]

REVISITING GLACE: UNDERSTANDING THE ROLE OF THE LAND SURFACE IN LAND-ATMOSPHERE COUPLING

WHS Corrected — WHS Uncorrected — IGBP Corrected — IGBP Uncorrected

$\Omega_P(S)-\Omega_P(W)$

Author names: Ruth Comer and Martin Best

Date: September 2011

WATCH is an Integrated Project Funded by the European Commission under the Sixth Framework Programme, Global Change and Ecosystems Thematic Priority Area (contract number: 036946). The WACH project started 01/02/2007 and will continue for 4 years.

Title:	Revisiting Glace: Understanding the Role of the Land Surface in Land-Atmosphere Coupling
Authors:	Ruth Comer and Martin Best
Organisations:	Met Office Hadley Centre
Submission date:	September 2011
Function:	This report is an output from Work Block 5
Deliverable	Contributes to WATCH deliverable 5.1. 4

1 Introduction

Soil moisture plays an important role in modifying the behaviour of the atmosphere by its influence on land surface fluxes of moisture, energy, carbon and trace gases (Seneviratne et al., 2010, and references therein). Of particular interest is the way in which the effects of these moisture and energy fluxes combine to create feedbacks on precipitation. Such feedbacks are complex due to their dependence on a variety of mechanisms.

The scarcity of observations of soil moisture and surface fluxes make it difficult to study these mechanisms in the real world. The mechanisms are difficult to detect even where observations do exist, since the relationship between soil moisture and precipitation is dominated by the latter's direct effect on the former (Guo et al., 2006). Many studies of the role of soil moisture therefore focus on the effects of soil moisture initialisation in a general circulation model (GCM; recent examples of such studies include Hohenegger et al., 2009, Koster et al., 2010, and Moufouma-Okia and Rowell, 2010). The advantage of this method is that soil moisture may be artificially prescribed, and the modelled effects on precipitation compared to the relatively more widely available atmospheric observations. A disadvantage is the problem of defining what the initial soil state should be, and whether the chosen values are realistic in the context of the particular model (note that there is no consistent definition of model soil moisture, Koster et al., 2009).

The Global Land-Atmosphere Coupling Experiment (GLACE; Koster et al., 2004, 2006; Guo et al., 2006) provided a framework for quantifying the influence of a GCM's soil moisture on its precipitation (and other atmospheric variables) using the model's own internal variability to define the range of soil moisture sampled. This gave a land-atmosphere coupling diagnostic which was independent of any assumptions about how soil moisture is modelled. Additionally, the test involved the prescription of soil moisture throughout a season rather than simply the starting conditions, as in other studies. This meant that the influence of soil moisture on precipitation could be measured through the season, without the complication of the precipitation feeding back on the soil moisture.

In the GLACE model intercomparison project, twelve models were compared and three "hot spot" regions were identified as having consistently strong coupling across most of the models: India, the Sahel region of Africa and the southern United States of America (Koster et al., 2004). That study also suggested a positive link between a model's land-atmosphere coupling strength and its skill in reproducing climatological mean precipitation (Koster et al., 2006). While the geographical distributions of the land-atmosphere coupling signals were largely consistent, the strength varied considerably across the models, with a few displaying very weak coupling. The weakest were the Australian Bureau of Meteorology Research Centre's Atmospheric Model (labelled BMRC), the National Centres for Environmental Prediction Global Forecast System (GFS) model coupled to the Oregon State University (OSU) land surface scheme (LSS), and the Met Office Hadley Centre's atmospheric model HadAM3.

Guo et al. (2006) divided the path of soil moisture-precipitation coupling into two segments, considering the influence of soil moisture on evaporation separately from the atmospheric response. They argued that strong land-atmosphere coupling requires three conditions: soil moisture must have a strong influence on evaporation, evaporation must have reasonably high variability and the atmosphere must respond to that evaporative variability. For the BMRC and GFS-OSU models, Guo et al. (2006) found that the soil moisture-evaporation segment of the coupling was weak, with the soil moisture having little control on evaporation in the GFS-OSU model, and evaporation variability being low for the BMRC model. Recently, Wei and Dirmeyer (2010) and Zhang et al. (2011) have revisited the GLACE analysis using an updated version of the GFS model, coupled to a much developed version of the OSU LSS, now known as Noah. They found that the GFS-Noah configuration still displays weak coupling, but that this can not be fully attributed to the Noah LSS. Using a second atmospheric model and two other LSSs, Wei and Dirmeyer (2010) tested six configuration pairings. They found that slightly stronger land-

atmosphere coupling was achieved by coupling the GFS model to a different LSS, but all three LSSs produced significantly stronger signal when coupled to the Centre for Ocean-Land-Atmosphere Studies's atmospheric model (COLA; also a more recent version of one of the original GLACE models, which was then ranked above average for land-atmosphere coupling strength). Thus the lack of land-atmosphere coupling in the original GFS-OSU model was likely to be partly caused by a lack of response by the atmosphere to the surface fluxes, as well as the weak control of soil moisture on evaporation.

In the HadAM3 case, Guo et al. (2006) found that the soil moisture-evaporation segment of the coupling was higher than average. They therefore attributed HadAM3's weak land-atmosphere coupling entirely to a lack of atmospheric response. Lawrence and Slingo (2005) explored this further, applying the GLACE method to two versions of HadAM3. One used HadAM3's standard configuration, and the other used hydraulic parameters which were chosen artificially in order to maximise the soil moisture's control on evaporation. They found negligible difference in the soil moisture-precipitation coupling diagnostic between the two cases, confirming that the weak coupling was likely due to the atmosphere's lack of response.

In the present study, we apply the GLACE method to a recent climate configuration of the Met Office Hadley Centre's atmospheric GCM, HadGEM3-A. Compared to HadAM3, our new model has increased horizontal and vertical resolution and incorporates updated parametrizations of the boundary layer and convection as well as a new dynamical core. We use a land surface configuration that is very similar to that used for HadAM3 in the original GLACE comparison, in order that any improvement in the coupling strength may be attributed to the new atmosphere. In addition to testing the coupling strength of the updated atmospheric model, we are also interested in how a change in the land surface scheme may affect the coupling strength, and therefore apply the method for several cases. Unlike the work of Wei and Dirmeyer (2010) and Zhang et al. (2011), we use the same LSS for each test case, but alter some key soil parameters. Our range of experiments therefore produce a smaller range of results, but this range should be easier to interpret, thereby contributing to our understanding of the mechanisms which control the coupling strength.

2 Experiment Setup

2.1 Model Configuration

HadGEM3 is the latest climate configuration of the Met Office Unified Model. It is a prototype model which is currently under development. Hewitt et al. (2011) provide a full description of the model's infrastructure and a scientific description of an early version (r1.1). In the current study, the atmospheric component (denoted HadGEM3-A) of a more recent version (r3.0) is used. This version predates that described by Walters et al. (2011) by about a year and does not include the large scale rain developments and the enhanced stratocumulus entrainment described therein, among other minor changes. The land surface scheme used here is MOSES-II (Essery et al., 2001). For consistency with the previous HadAM3 GLACE studies (Koster et al., 2006; Lawrence and Slingo, 2005), the land surface hydraulic scheme is based on that of Clapp and Hornberger (1978). Hydraulic parameters are calculated using the Cosby et al. (1984) equations and soil texture properties from two datasets, described below. Two aspects of the land surface configuration used here are different from the Essery et al. (2001) parametrizations used in HadAM3: the soil thermal conductivity is a simplified version of Johansen (1975) presented by Dharssi et al. (2009) and the interception of light for plant photosynthesis is calculated using the multi-layer canopy radiation scheme of Mercado et al. (2007). The model uses a regular latitude-longitude grid in the horizontal (1.875° in longitude by 1.25° in latitude for this experiment) and the present configuration uses the standard four layers in the land surface (Cox et al., 1999) but 85 vertical levels in the atmosphere. These extend the atmosphere to 85km, covering the entire stratosphere (Hewitt et al., 2011) as well as providing increased resolution in the boundary layer

and free troposphere (see Senior et al., 2011, for a review of the advantages of increased vertical resolution).
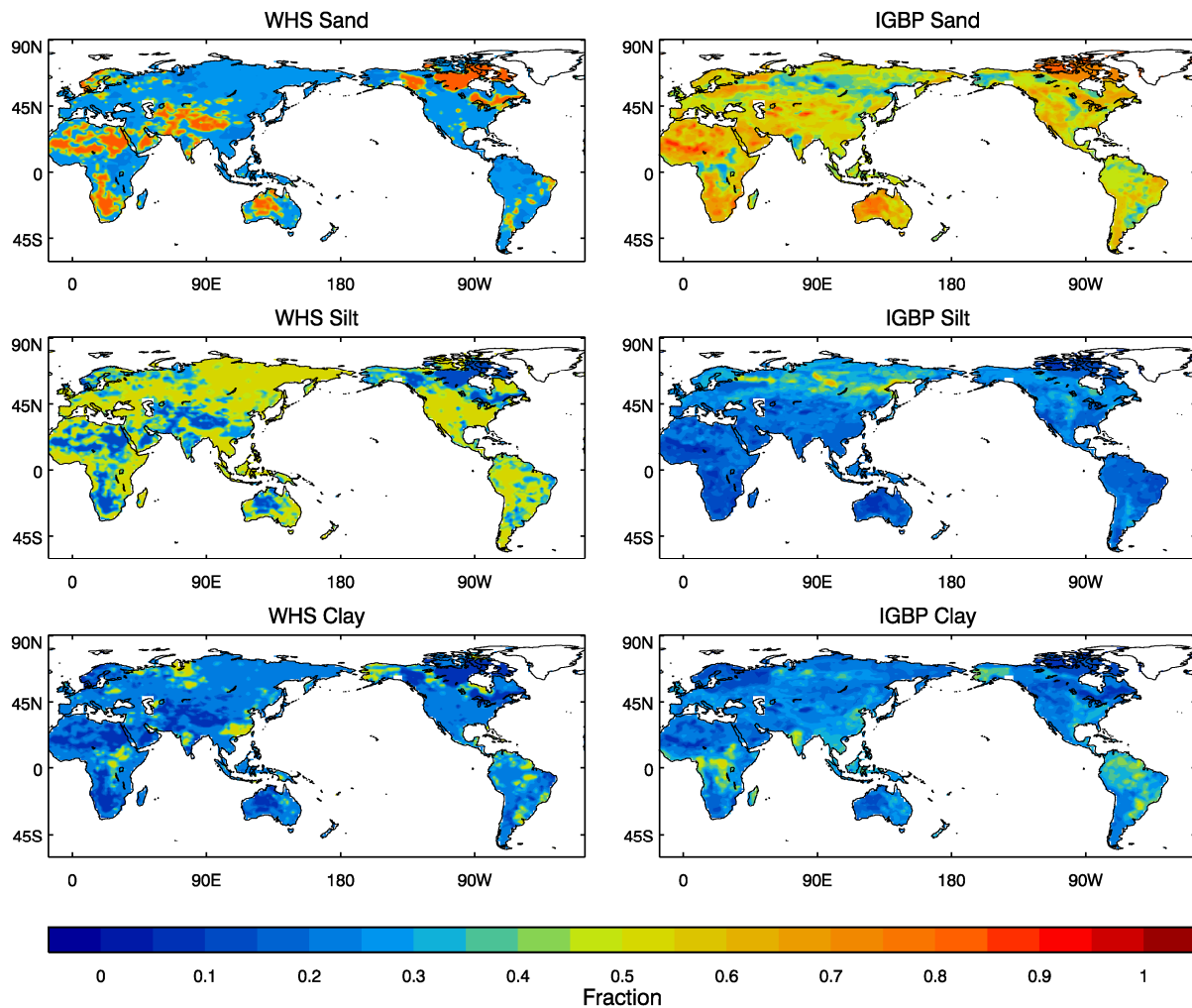
Figure 1: Fractions of soil texture classes used to calculate Clapp and Hornberger (1978) parameters from WHS (left) and IGBP (right).

Datasets used for the Cosby et al. (1984) calculations are as follows: (i) the data described by Wilson and Henderson-Sellers (1985) and used in the HadAM3 configuration, hereafter referred to as WHS; (ii) a more recent dataset available from the International Geosphere-Biosphere Programme Data and Information System (IGBP-DIS; Global Soil Data Task, 2000) and assessed for use in the Unified Model by Dharssi et al. (2009). The IGBP data have far higher resolution than the WHS (5 arc-minutes compared to 1˚) so should provide a more realistic, smoothly varying field at the resolution of the HadGEM3-A model. Figure 1 shows the fractions of sand, silt and clay from each of these data sets at the resolution of the model. Figure 1 shows that the IGBP texture map (right) is indeed smoother than the older WHS map (left). There is also a clear discrepancy between the designation of sand and silt fractions, with far more sandy soils for the IGBP data set over most of the globe, but a lower sand fraction in the regions that WHS designate as sandy. These widespread high values of sand in the IGBP data were thought to be unrealistic (Dharssi et al., 2009) and this data set was therefore not included in the further HadGEM3 development. However, they still provide a useful test case for understanding the link between soil parameters and land-atmosphere interactions.

Recently, an error was found in the way that the Cosby et al. (1984) equations were applied in the Unified Model ancillary file creation system. The correction of this error increased the limits of the range

of soil moisture concentrations under which plants experience stress (the critical point, θ_c, and wilting point, θ_w) as well as increasing the range of this stress region ($\theta_c - \theta_w$; Section 4 has more detail about how these parameters are applied in the Unified Model, and Section 5 about their calculation). This led to a general reduction of evaporation from the land surface (Dharssi et al., 2009; Compton, 2008), and it was hypothesised that the greater range of the stress region could lead to a stronger land-atmosphere coupling strength. With this in mind, this report investigates four experiment cases, identical except for the hydraulic parameters. The four cases are: WHS based properties with and without the correction, IGBP based properties with and without the correction.

2.2 GLACE Framework

The GLACE framework is described fully by Koster et al. (2006). The method works by assessing the difference between two ensembles of runs for a given GCM. In the first ensemble, the soil moisture is allowed to vary freely, according to the model's prognostic equations. In the second, the soil moisture is prescribed. In geographical regions where soil moisture is an important factor in the model's atmospheric evolution, a difference between the two ensembles should be evident in the atmosphere's diagnostics.

Each ensemble consists of sixteen model runs which each run for three months from 1st June 1994. Sea surface temperatures (SSTs) are prescribed using observations from the Atmospheric Model Intercomparison Project (AMIP) II dataset (Gates et al., 1999). Within each ensemble, the runs differ only in their initial conditions. In the present study these starting conditions were created as follows: HadGEM3-A was run for sixteen years. This time the SSTs were prescribed using AMIP data averaged for each month over the period 1978-1994, so that they varied seasonally but not interannually. From this longer run, the model prognostic variables from the beginning of June each year were saved and used to initialise the sixteen short runs. This approach is consistent with option (iii) in the hierarchy of methods suggested in Appendix A of Koster et al. (2006).

In the control ensemble (labelled "W" for write) each run is allowed to progress normally. From one of the runs in this ensemble (labelled "W1", although the choice of run is arbitrary), the soil moisture prognostic variable is written to a file after every timestep and saved for use in the second ensemble. In the second ensemble ("S"; prescribed soil moisture), the soil moisture prognostic variable is discarded at the end of every timestep, and the W1 soil moisture from the relevant timestep is read in. In this way, the evolution of soil moisture is forced to be the same for every run in the S ensemble. Note that the method as described by Koster et al. (2006) defines the S ensemble by prescribing only the soil moisture in subsurface layers, which they define as soil layers with their central depth at five centimetres or below. Since the top layer of MOSES-II is ten centimetres thick, these descriptions are equivalent for our purposes (Lawrence and Slingo, 2005, took the same approach). Five models (including HadAM3) in the original GLACE intercomparison had a land surface scheme with a top layer of at least ten centimetres thick. The only one of these where the top layer soil moisture in the S ensemble was not prescribed was the GFS/OSU model (Guo et al., 2006). This model also displayed very weak land-atmosphere coupling, which Zhang et al. (2011) have partly attributed to the unusual significance of the top layer for transpiration in the OSU scheme.

To assess the influence of soil moisture on a given atmospheric variable, v, the "similarity diagnostic", Ω_v, is calculated for each of the W and S ensembles. Ignoring the first eight days, six day averages are calculated for each grid cell in the domain, giving sixteen time series with fourteen entries each. Then

$$\Omega_v = \frac{16\hat{\sigma}_v{}^2 - \sigma_v{}^2}{15\sigma_v{}^2},$$

(1)

where $\hat{\sigma}_v$ is the standard deviation of the mean time series for the grid cell (i.e. the 14 values obtained from averaging across the ensemble), and σ_v is the standard deviation across the 16 time series (i.e. the standard deviation of the 16 × 14 values). Ω_v therefore varies between 0 and 1, where sixteen identical time series would give $\Omega_v = 1$. The coupling diagnostic is simply the difference between the similarity in the two ensembles, $\Omega_v(S) - \Omega_v(W)$. Higher values of this coupling diagnostic indicate that soil moisture provides a constraint on the atmospheric variable, v.
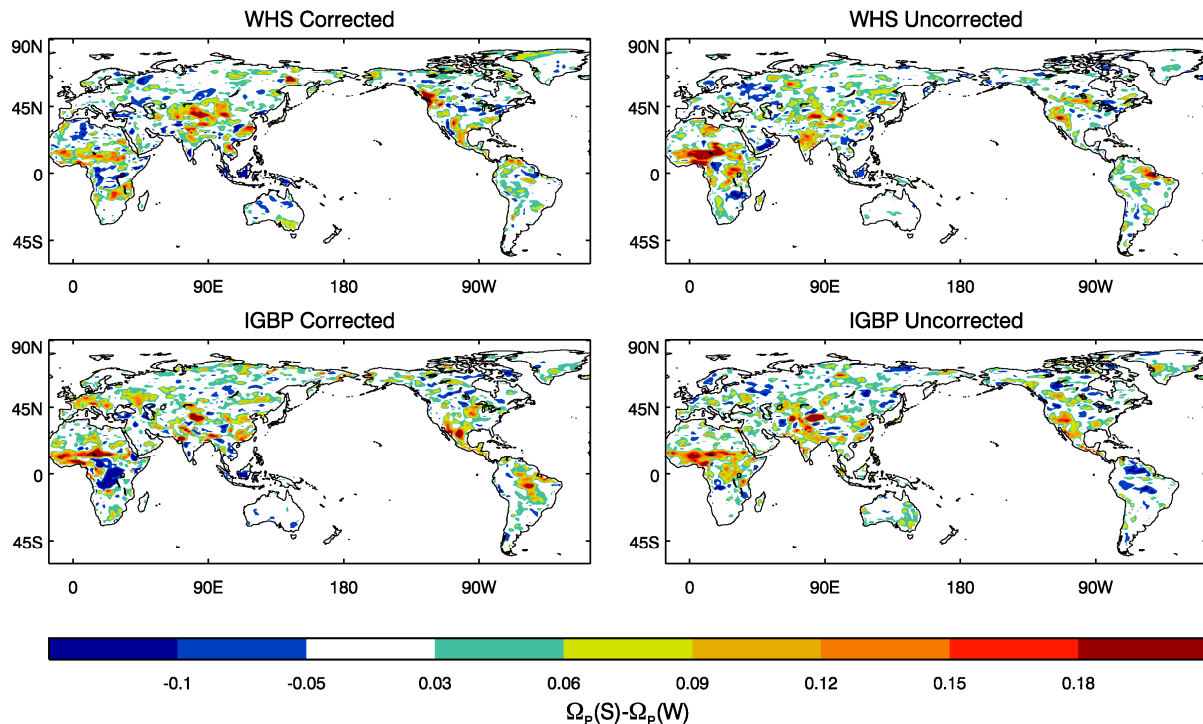
Figure 2: Measured HadGEM3-A influence of soil moisture on precipitation using corrected (left) and uncorrected (right) WHS (upper) and IGBP (lower) soil properties.

3   HadGEM3-A Coupling Strength

Figure 2 shows the GLACE coupling diagnostic for precipitation $\Omega_P(S) - \Omega_P(W)$ for the four cases described in Section 2.1. Red colours indicate areas where precipitation is strongly influenced by soil moisture. In all four cases, the coupling is stronger than that in the previous HadAM3 experiment (Koster et al., 2006, Fig. 5). This is particularly clear over the Sahel region of Africa, and to a lesser extent over the southern United States of America. Regional differences exist between the four cases, with the strongest signals for the Sahel appearing in the "WHS uncorrected" and "IGBP corrected" cases. This is somewhat counter-intuitive, since one might expect the effect of the correction to be consistent between the IGBP and WHS datasets.

The land surface parametrization in the "WHS uncorrected" case is very similar to that used in HadAM3. It is therefore reasonable to infer that the stronger coupling found here is due to developments in the atmospheric component of the model. This result is consistent with the findings of Guo et al. (2006) and Lawrence and Slingo (2005), discussed in the introduction. Those studies argued that the weak coupling in HadAM3 was due to the atmosphere's lack of response to variations in the land surface evaporation, rather than the land surface's ability to control evaporation.
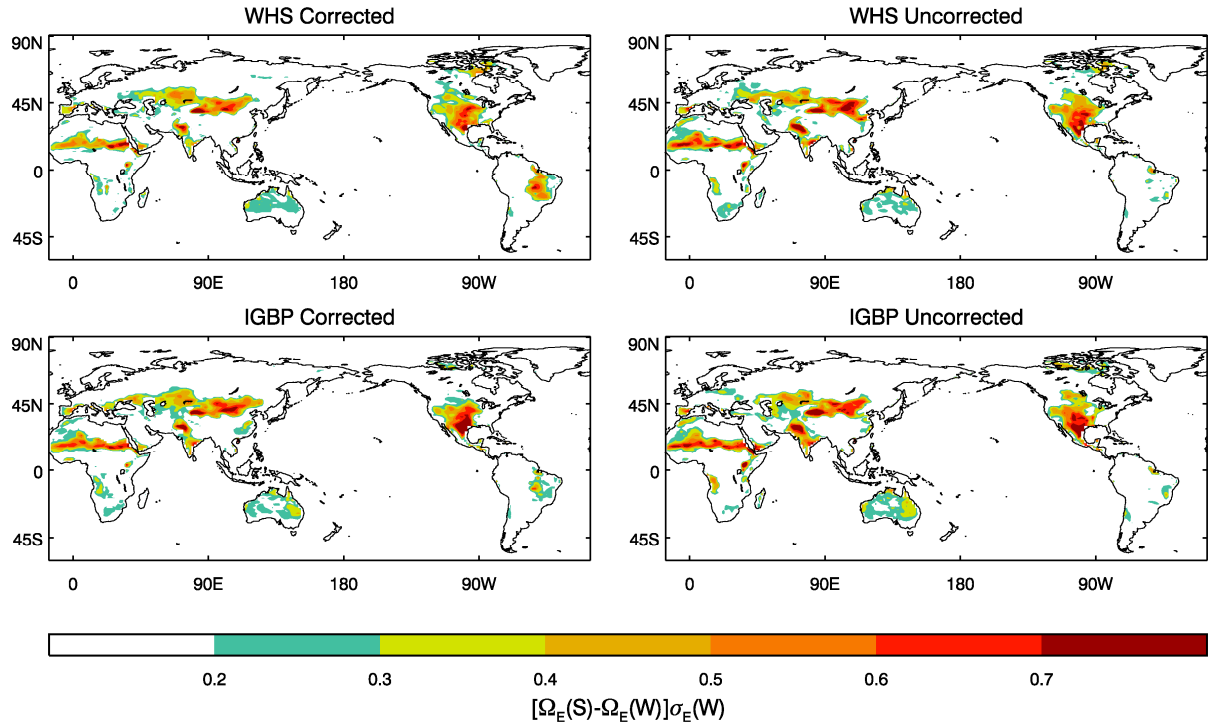
Figure 3: **As Figure 2, but for soil moisture influence on surface evaporation (*E*), scaled by the standard deviation of *E* in the control (W) ensemble.**

To understand better the spread of coupling strengths found across the models compared by Koster et al. (2006), Guo et al. (2006) also measured the soil moisture's effect on land surface evaporation in each case. They argued that for the atmosphere to respond to the soil moisture, the evaporation must satisfy two conditions: evaporation must be influenced by soil moisture, and evaporation must be sufficiently variable to influence the atmosphere. The GLACE evaporation coupling diagnostic for each model was therefore scaled by the standard deviation of surface evaporation from the control (W) ensemble ($[\Omega_E(S) - \Omega_E(W)]\sigma_E(W)$ see Guo et al., 2006 Fig. 5). HadAM3's diagnostic had above average coupling strength by this measure: Guo et al. (2006) ranked the models according to the areal average of both the soil moisture-precipitation coupling diagnostic, $SM \rightarrow P$, and the scaled soil moisture-evaporation coupling diagnostic $SM \rightarrow E$, i.e.

$$SM \rightarrow P = \overline{\Omega_P(S) - \Omega_P(W)} \qquad (2)$$

$$SM \rightarrow E = \overline{[\Omega_E(S) - \Omega_E(W)]\sigma_E(W)} \qquad (3)$$

HadAM3 was ranked 11th for the former and 6th for the latter (Guo et al., 2006, Table 1), leading to the conclusion that HadAM3's weak coupling was due to the atmosphere's lack of response to evaporation variability. Figure 3 shows the equivalent diagnostic for the four HadGEM3-A cases (here and throughout the report "evaporation" or "*E*" in HadGEM3-A refers to the total of bare soil evaporation and plant transpiration). This time the maps appear very similar to the HadAM3 case, which is further evidence that the stronger coupling in HadGEM3-A compared to HadAM3 is due to the atmospheric, rather than the land surface, component. The differences between these maps are discussed in detail in Sections 5 and 6. Here we simply note that, according to this diagnostic, the correction to the Cosby et al. (1984) algorithm decreases the land-atmosphere coupling over the Sahel for both WHS and IGBP cases. The counter-intuitive result noted above for the soil moisture-precipitation diagnostic in this region is therefore not explained by the evaporation effects.

This result, and the general noisiness of the patterns in Figure 2 compared to Figure 3 may be attributed to the complex nature of the land surface's influence on precipitation. An anomaly in soil

moisture may produce a positive or a negative response in the precipitation, depending on the atmospheric profile (Findell and Eltahir, 2003): A wet soil anomaly may increase evaporation, leading to a moister atmosphere with increased CAPE, thereby stimulating an increase in convection. A dry soil anomaly may increase sensible heat flux, leading to a deeper boundary layer. If this deeper boundary layer extends to the level of free convection, it could trigger convection in an otherwise stable atmosphere. Due to advection, the influence of soil moisture on precipitation may be non-local, with effects occurring downstream of soil moisture anomalies (e.g. Beljaars et al., 1996). The circulation itself may also be affected by soil moisture, producing further non-local effects (e.g. Taylor, 2008). Seneviratne et al. (2010) has a comprehensive review of these interaction studies.

For completeness, Table 1 presents global summary statistics for the coupling diagnostic using the definitions of Guo et al. (2006). Globally, the coupling is weakened by the correction to the Cosby equations using either IGBP or WHS soil data, and the coupling using WHS data is weaker than that using IGBP data. For all four cases, the $SM \rightarrow E$ value is higher than that for HadAM3. This difference can not be fully attributed to the remaining differences in the land surface scheme: further tests (not shown) using the Cox et al. (1999) parametrizations of soil thermal conductivity and plant canopy light interception adjusted the $SM \rightarrow E$ values by approximately +0.002 and −0.003 respectively. There is a possible indirect effect: land surface evaporation is partly controlled by near surface atmospheric variables such as temperature and humidity, as well as incident radiation. Since the atmosphere in HadGEM3-A is more strongly influenced by the land than in HadAM3, the constraints on the atmospheric variables may feed back into an additional constraint on the evaporation. Further, Wei and Dirmeyer (2010) pointed out that two different atmospheric models coupled to the same land surface scheme can produce significantly different soil moisture variability. By swapping the saved W1 soil moisture between two GLACE cases with the same LSS but different atmospheres, they demonstrated that the nature of this variability alone has an impact on the GLACE coupling diagnostic.

Experiment	$SM \rightarrow P$	$SM \rightarrow E$
WHS Corrected	0.010	0.135
WHS Uncorrected	0.016	0.142
IGBP Corrected	0.015	0.139
IGBP Uncorrected	0.018	0.152
HadAM3 (from Guo et al., 2006)	0.002	0.129

Table 1: Summary statistics of coupling strength for the four experiments (c.f. Table 1 of Guo et al., 2006). See text for details.

Despite the differences noted above in the patterns of Figures 2 and 3, the rankings of the statistics in Table 1 demonstrate that the global picture is consistent between these two land-atmosphere coupling diagnostics. The details of the precipitation's response are beyond the scope of the current study, but will be a subject of future work. The remainder of this report focuses on the scaled soil moisture-evaporation coupling diagnostic, since it is better constrained and therefore more useful for understanding the differences caused by the different land surface properties in our four experiments.

4 Controls on Coupling

The diagnostic in Figure 3 may best be understood by separating it into its two factors, the soil moisture's influence on evaporation ($\Omega_E(S) - \Omega_E(W)$) and the evaporation variability ($\sigma_E(W)$). Figure 4 shows maps of the former for each of the four experiment cases. In the Unified Model, transpiration (which dominates the evaporation signal) is modulated by the soil moisture availability factor, β (Cox et al., 1999; Essery et al., 2001):

$$\beta_i = \begin{cases} 1 & \text{if } \theta_i \geq \theta_c \\ \dfrac{\theta_i - \theta_w}{\theta_c - \theta_w} & \text{if } \theta_w < \theta_i < \theta_c \\ 0 & \text{if } \theta_i \leq \theta_w \end{cases} \tag{4}$$

where θ_i is the volumetric soil moisture for soil layer i, θ_w is the soil moisture content at the wilting point and θ_c is the soil moisture content at the critical point. θ_w and θ_c are fixed using values read in from the ancillary file created using the Cosby et al. (1984) equations (see Sections 2.1 and 5).
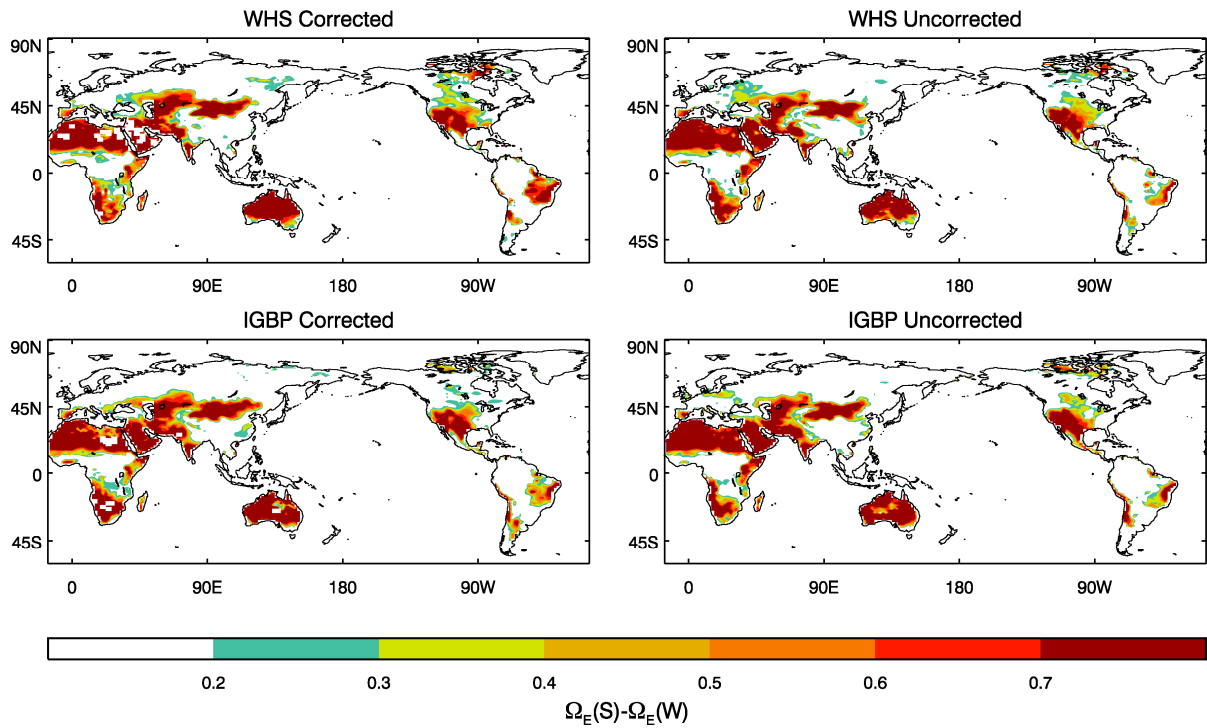
Figure 4: As Figure 2, but for soil moisture influence on surface evaporation (E).

When $\beta_i = 0$, no moisture is taken from soil layer i; when $\beta_i = 1$, moisture uptake from layer i is not limited by soil moisture amount. Then, transpiration rates are limited by plant physiology (which in turn is influenced by atmospheric variables such as near surface temperature, pressure and air composition) and light levels (see Appendix A of Cox et al., 1999). It is therefore to be expected that soil moisture-evaporation coupling will be highest in regions where overall β is lowest. This is confirmed for the majority of the globe by figure 5, which shows the average β from the control (W) ensemble. Here and in later figures, β is taken as the sum over the four soil layers, weighted by the plant root fraction in each layer:

$$\beta = \sum_i \beta_i \sum_j p_j r_{ij} \tag{5}$$

where p_j is the fraction of the grid cell covered by the j th plant type and r_{ij} is the corresponding root fraction in the i th soil layer (calculated according to Equation 32 and Table 6 of Essery et al., 2001). The dryest (low β) areas in Figure 5 are clearly consistent with the strong coupling areas of Figure 4, and the moist (high β) areas are consistent with the weak coupling regions. This relationship appears to break down in parts of northern Russia and Canada, where low β is not accompanied by strong soil

moisture-evaporation coupling. Since β is calculated using a weighting by plant type (Equation 5) and not normalised by total vegetation cover, sparsely vegetated regions such as these will show low β values even though soil moisture is plentiful (not shown).
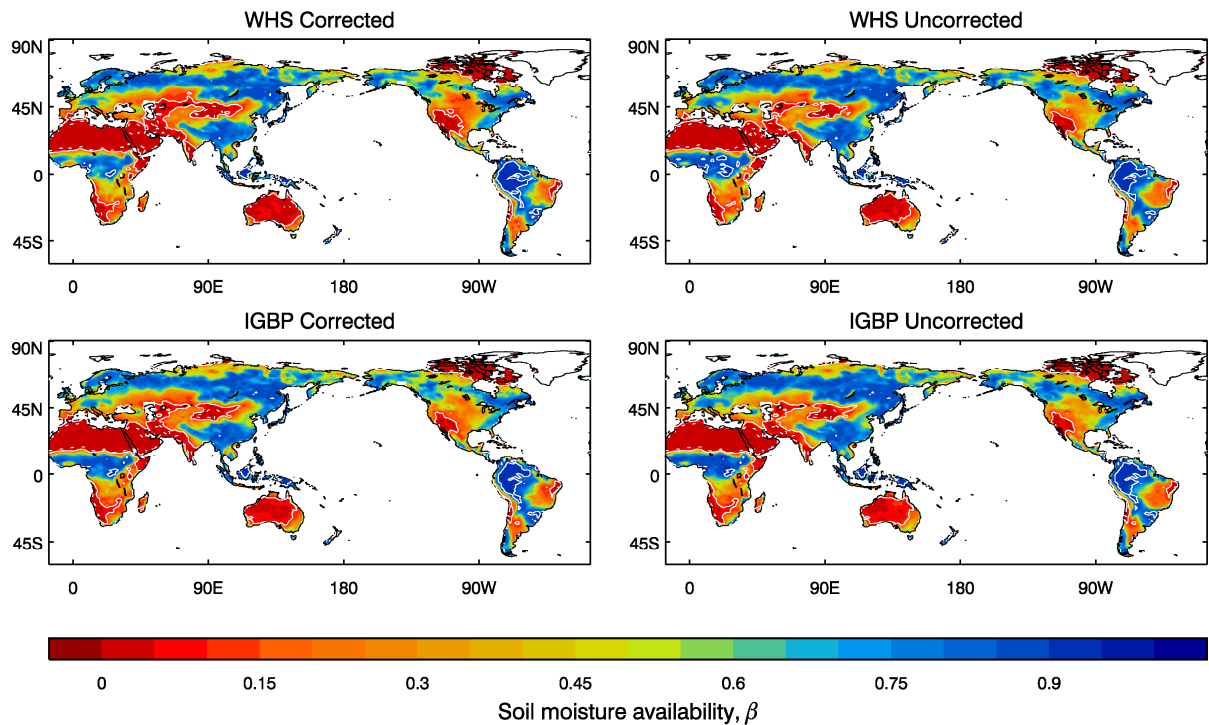
Figure 5: As Figure 2, but for soil moisture availability factor, β averaged over the control (W) ensemble. White isolines at 0.01 (dashed), 0.1 and 0.9 (solid) delineate very dry, dry and wet regions respectively.

Figure 6 (left) further illustrates this relationship for the tropics and mid-latitudes. It shows $\Omega_E(S) - \Omega_E(W)$ plotted against the mean β from the control (W) ensemble. Each point represents a grid cell between 60°N and 60°S. Data from the different experiments are plotted in different colours, but there is no discernable difference in the spread of points.

Although there are many influences on evaporation through meteorology and plant physiology, Fig. 6 (middle) shows a clear dominant influence of moisture availability. There is also a strong correlation between the mean and standard deviation of evaporation (Fig. 6, right).
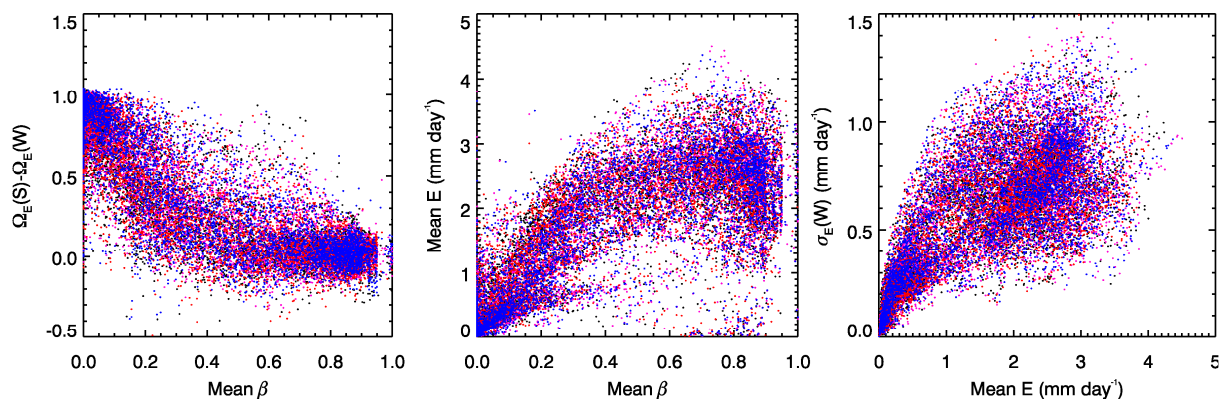
Figure 6: Soil moisture-evaporation coupling against W ensemble mean β (left); evaporation (E) mean against β mean (middle); E standard deviation against E mean (right). Each point represents a grid cell between 60°N and 60°S for the corrected WHS (black) and IGBP (red), and uncorrected WHS (magenta) and IGBP (blue) experiments.
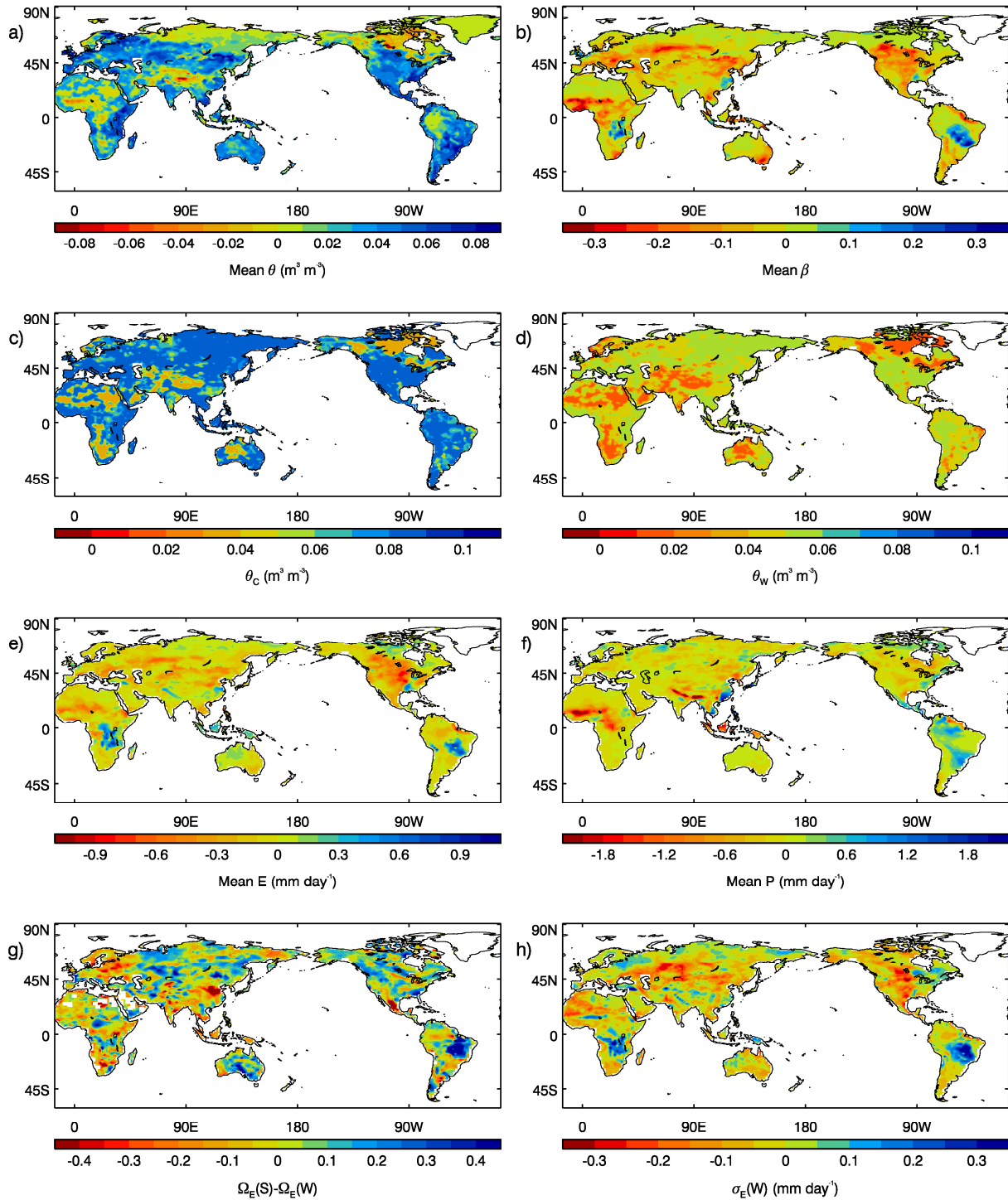
Figure 7: Difference maps (corrected - uncorrected) for variables from the WHS experiments: a) mean total column soil moisture; b) mean soil moisture availability factor; c) soil moisture at critical point; d) soil moisture at wilting point; e) mean evaporation; f) mean total precipitation; g) soil moisture-evaporation coupling; h) evaporation standard deviation. Means and standard deviations are based on six day averages from the W ensemble.

5 Effect of Ancillary Correction

Figure 7 shows difference maps "corrected-uncorrected" for some key variables from the experiments. Where a difference between means or standard deviations is shown, these are calculated from the 14×16 six day averages from the control (W) ensemble (and therefore consistent with the calculation

of Ω_v). The results presented here are from the WHS experiments, but similar results were found with the IGBP experiments. Figure 7a shows the changes in total column volumetric soil moisture due to the correction. The pattern of changes corresponds to the distribution of soil textures, with decreases in areas which are dominated by sand, and increases elsewhere (Figure 1, top left). Some parts of the high latitudes, central Africa and the north-west of South America show little change because soil moisture is close to saturation. The sand fraction plays a significant role in the speed of drainage through the soil, which in the UM is calculated by the Darcy equation (Cox et al., 1999):

$$W = K\left(\frac{\partial \Psi}{\partial z} + 1\right) \tag{6}$$

W is the flux of moisture in the downward (z) direction, K and Ψ are the soil hydraulic conductivity and suction calculated according to the equations of Clapp and Hornberger (1978):

$$K = K_s\left(\frac{\theta_{uf}}{\theta_s}\right)^{2b+3} \tag{7}$$

$$\Psi = \Psi_s\left(\frac{\theta_{uf}}{\theta_s}\right)^{-b} \tag{8}$$

where θ_{uf} is the unfrozen soil moisture fraction. K_s, Ψ_s and θ_s are the hydraulic conductivity, suction and volumetric moisture at saturation. These and the Clapp-Hornberger b parameter are all calculated according to the equations of Cosby et al. (1984):

$$K_s = \begin{cases} 0.007(10^{-0.6-0.64f_c+1.26f_s}) & \text{(Corrected)} \\ 0.007(e^{-0.6-0.64f_c+1.26f_s}) & \text{(Uncorrected)} \end{cases} \tag{9}$$

$$\Psi_s = \begin{cases} \dfrac{10^{2.17-0.63f_c-1.58f_s}}{100} & \text{(Corrected)} \\[4mm] \dfrac{e^{2.17-0.63f_c-1.58f_s}}{100} & \text{(Uncorrected)} \end{cases} \tag{10}$$

$$\theta_s = 0.505 - 0.037f_c - 0.142f_s \tag{11}$$

$$b = 3.10 + 15.70f_c - 0.3f_s \tag{12}$$

where f_c and f_s are the fractions of clay and sand, as displayed in Figure 1. K_s and Ψ_s are both calculated differently in our two cases, but the change in K_s dominates the effect on Equation 6 since its effect does not depend on the soil moisture profile and its relative change with the correction is large. Figure 8 (left) shows the ratio of K_s between the corrected and uncorrected cases. In sandy regions it is increased (due to positive exponents in Equation 9) by approximately 75% and elsewhere it is decreased (negative exponents) by around 50%. Therefore drainage through the soil is increased for sandy regions (drying the soil) and decreased over the rest of the world (moistening the soil).
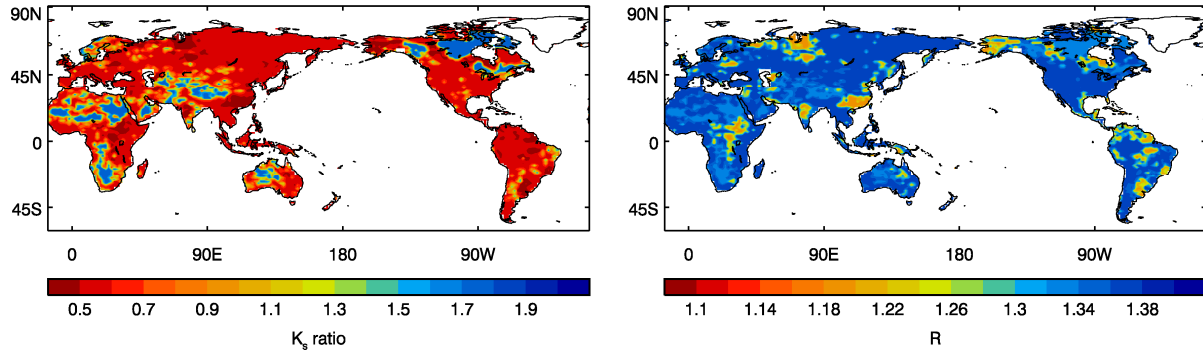
Figure 8: Ratio of corrected to uncorrected soil parameters for WHS case: ratio of hydraulic conductivity at saturation (left) and R (Equation 15; right).

The increase in soil moisture over most of the globe does not translate into an increase in moisture availability to plants (β; Fig. 7b) for most regions. This is explained by the increases in θ_w and θ_c (Fig. 7c,d) and their difference (not shown) which decrease β directly through Equation 4. θ_c and θ_w are calculated from the Clapp and Hornberger (1978) equations:

$$\theta_c = \theta_s \left(\frac{\Psi_s}{\Psi_c} \right)^{\frac{1}{b}} \tag{13}$$

$$\theta_w = \theta_s \left(\frac{\Psi_s}{\Psi_w} \right)^{\frac{1}{b}} \tag{14}$$

where Ψ_c = 3.364m and Ψ_w = 152.9m are the soil suction at the critical and wilting point respectively. Note that the relative changes in θ_w, θ_c and $\theta_c - \theta_w$ are all equal and

$$\frac{\theta_w^c}{\theta_w^u} = \frac{\theta_c^c}{\theta_c^u} = \frac{\theta_c^c - \theta_w^c}{\theta_c^u - \theta_w^u} = \left(\frac{\Psi_s^c}{\Psi_s^u} \right)^{\frac{1}{b}} = R \tag{15}$$

where the superscripts c and u denote the corrected and uncorrected cases. This quantity is displayed in Figure 8 (right). The increase due to the correction ranges between 19% and 37% and is highest in regions with a high proportion of silt (where the exponents in Equation 10 are maximised), and lowest in regions with a high proportion of clay (where b is maximised, Eq. 12; c.f. Figure 1, left). In stressed regions (where θ lies between θ_w and θ_c), β will increase with the correction where $\frac{\theta^c}{\theta^u} > R$ and decrease where $\frac{\theta^c}{\theta^u} < R$.

Very few regions show an increase in β due to the correction (Fig. 7b). The most significant areas which do are in southern Africa and Brazil. To understand the increases here, we consider the annual cycles of precipitation and soil moisture, which are strong in these regions due to the annual procession of the inter-tropical convergence zone. Figure 9 shows these for the southern African region, (taking an average over the box 22˚-32˚E, 10˚-18˚S). Similar results (not shown) were found for the Brazilian region. Soil moisture is only shown for layers 2 and 3, since these layers dominate the vegetation root-zone (and therefore the β signal, Equation 5) for this region. The vertical dashed line marks the start of the control (W) ensemble data (JJA). Data from September to May are taken from the sixteen-year run which generated the ensemble starting conditions for each case (Section 2.2). The horizontal dashed lines on the four soil moisture panels indicate the soil moisture fractions at wilting, critical and saturation points.
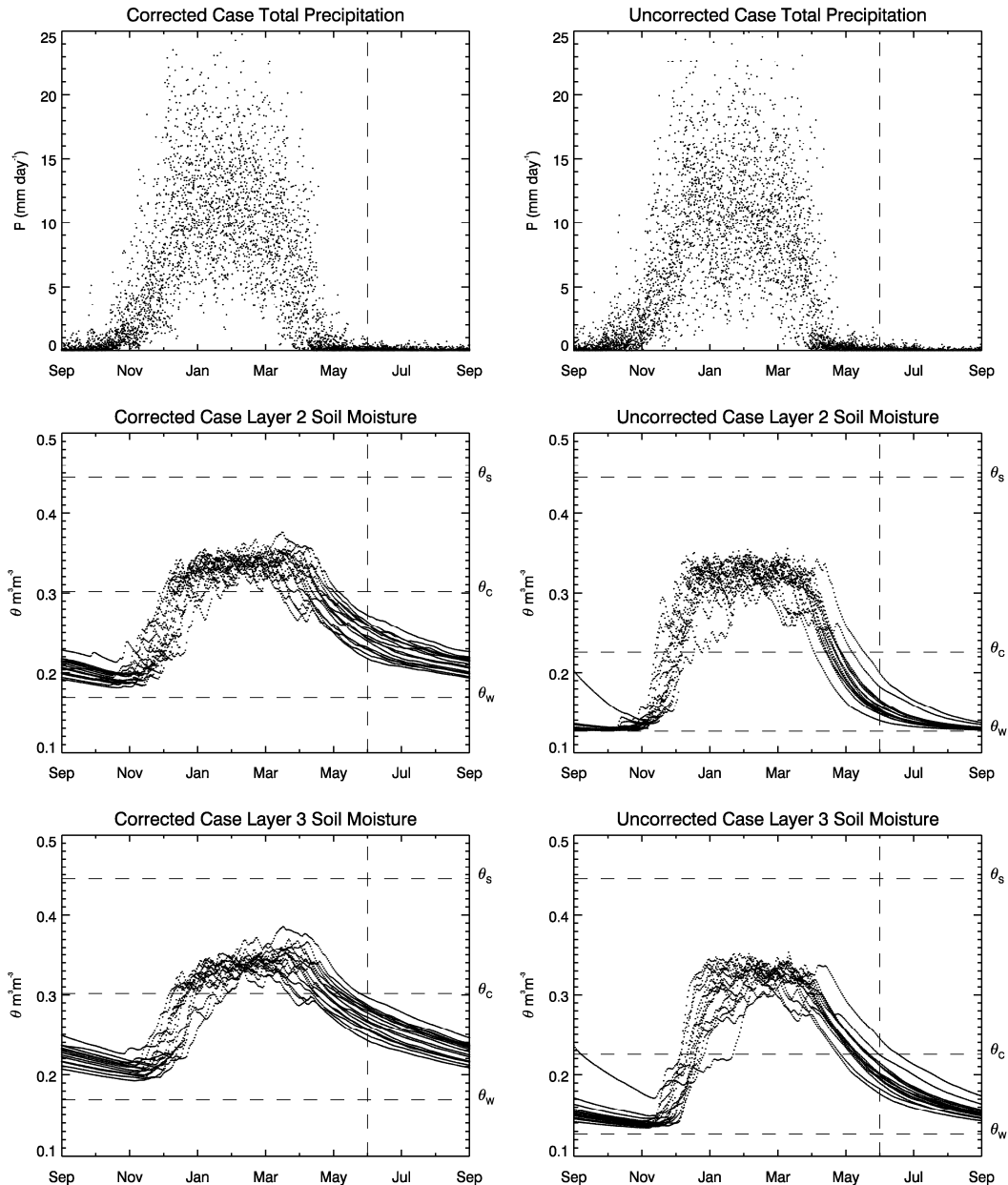
Figure 9: Southern Africa daily averaged precipitation (upper) and layer 2 (middle) and 3 (lower) soil moisture fraction for corrected (left) and uncorrected (right) cases. September-May data are from the sixteen-year run used to generate the ensemble starting conditions and June-August data are from the control (W) ensemble. The horizontal lines indicate the soil moisture fraction at critical, wilting and saturation point. All quantities are averaged over the region 22°-32°E, 10°-18°S.

The annual cycle of precipitation (Fig. 9 upper) is very similar between the two cases. It increases steadily through the spring (SON), maintains a maximum (albeit with large interannual variability) during the summer (DJF) and decreases through the autumn (MAM). There is very little precipitation during JJA (the GLACE ensemble period). The annual cycle in soil moisture closely follows that of precipitation. In the uncorrected case (right), soil moisture increases between September and November to reach a maximum during December for both soil layers. This maximum is maintained until late March, indicating that an equilibrium has been reached between the infiltration of moisture due to precipitation, and the loss via drainage and evaporation. From April, the soil moisture fraction decreases almost

asymptotically towards the wilting point, reaching a minimum at the end of August for layer 2 and during November for layer 3.

The annual cycle of soil moisture for the corrected case (left) has a smaller range, and the fraction continues to increase (very slowly) throughout the wet season. Since this region has a relatively low sand fraction (Figure 1, upper left), the correction gives a decrease in hydraulic conductivity (assuming the same soil moisture fraction), as discussed above (Equations 7 and 9 and Figure 8, left). The resulting smaller vertical moisture fluxes (Equation 6) slow both the increase in October-March and the decrease from April onward. This slower decrease from a similar maximum in April is responsible for the higher soil moisture during the GLACE ensemble period (JJA). Despite the higher critical and wilting thresholds (θ_w and θ_c, dashed horizontal lines) in the corrected case, inspection of the JJA period in the four soil moisture panels of Figure 9 shows that the soil moisture is increased with the correction even when considered relative to the relevant θ_w and θ_c .

Southern Africa and Brazil are the only regions where the strong precipitation annual cycle with a JJA dry season coincides with low sand-content soils and enough vegetation to produce a significant negative signal in β. All of the changes to β shown in Figure 7b produce corresponding changes in evaporation (Fig. 7e). Of course, these changes in surface evaporation feed back onto the soil moisture amount through a change in its water loss to the atmosphere.

A decrease in total precipitation is also visible over most of the world (Fig. 7f). This could most simply be explained by a reduction in the atmospheric moisture made available by evaporation. It should be noted, however, that evaporative effects on precipitation are in reality far more complicated (see Section 3). Increases in precipitation can be seen in South America and South-East Asia, most likely due to changes in the large scale circulation. These changes in precipitation across the globe feed back onto the soil moisture and, through β, the evaporation.

The coupling of evaporation to soil moisture is generally higher with the correction than without, although the pattern is quite noisy (Fig. 7g). This can be explained by the almost global decrease in β (Fig. 7b c.f. Fig. 6 left). The anomalous increase over eastern Brazil appears to be due to a change to the variability of soil moisture, rather than its average. In this region, the prescribed soil moisture ensembles for both the corrected and uncorrected cases show high evaporation similarity. i.e. $\Omega_E^c(S) \approx \Omega_E^u(S) > 0.95$, suggesting that the control of soil moisture on evaporation for both cases is about as high as may be measured by this method. The increase therefore comes from a decrease of evaporation similarity in the control ensemble:

$$\Delta[\Omega_E(S) - \Omega_E(W)] = [\Omega_E^c(S) - \Omega_E^u(S)] - [\Omega_E^c(W) - \Omega_E^u(W)] \qquad (16)$$
$$\approx -[\Omega_E^c(W) - \Omega_E^u(W)]$$

In the uncorrected W ensemble, the similarity of both E and β is high in this region, suggesting that soil moisture is not sampling a wide enough range of values to produce a measured influence on evaporation.

Since the variability of evaporation is closely related to its mean (Fig. 6, right), the pattern of change in $\sigma_E(W)$ is very similar to the pattern of change in the mean (Fig 7e,h). In general, this means a decrease in variability over most of the globe. The almost global decrease in β therefore has two competing effects on the overall coupling diagnostic $[\Omega_E(S) - \Omega_E(W)]\sigma_E(W)$: $\Omega_E(S) - \Omega_E(W)$ increases, and $\sigma_E(W)$ decreases. The significance of the change in each factor depends on the magnitude of the other factor (e.g. a large change in $\Omega_E(S) - \Omega_E(W)$ will have no impact if $\sigma_E(W) = 0$). Figure 10 therefore shows the difference in each factor from Figure 7g,h multiplied by the average of the other factor. i.e.

$$\Omega_E(S) - \Omega_E(W) \text{ contribution} = (A^c - A^u)\frac{B^c + B^u}{2}$$

$$\sigma_E(W) \text{ contribution} = (B^c - B^u)\frac{A^c + A^u}{2} \tag{17}$$

$$\text{where}$$

$$A = \Omega_E(S) - \Omega_E(W)$$

$$B = \sigma_E(W)$$

Note that the sum of these two maps is the same as the difference between the upper maps in Figure 3, and the sum of the areal averages is close to[1] the difference between $SM \rightarrow E$ for the WHS cases shown in Table 1. Figure 10 demonstrates that the change in the variability of evaporation is the dominant effect on the coupling diagnostic, and is responsible for the general reduction in land-atmosphere coupling strength noted in Section 3.
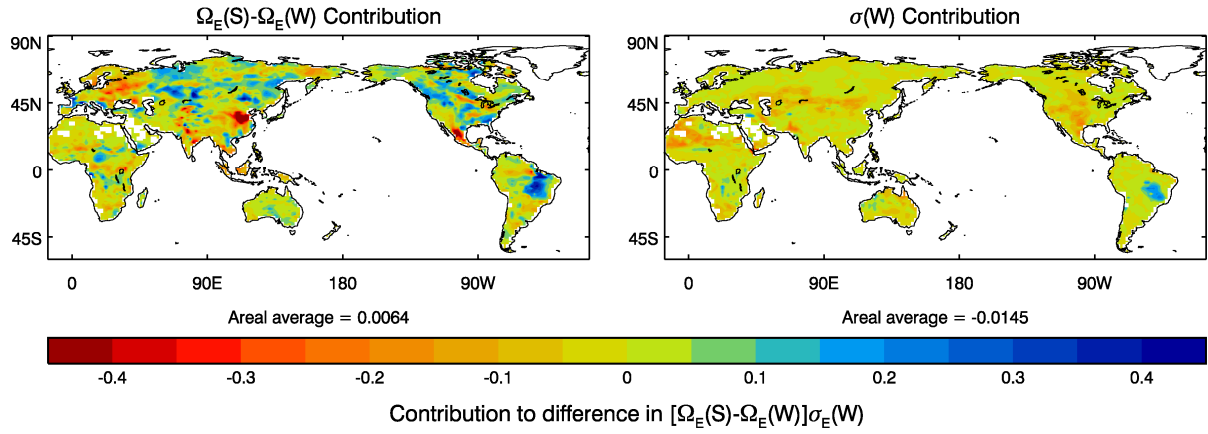
Figure 10: Difference (corrected-uncorrected using WHS data) in scaled soil moisture-evaporation coupling diagnostic, $[\Omega_E(S) - \Omega_E(W)]\sigma_E(W)$, divided into contributions from each factor. See text for details.

6 Effect of Soil Data Source Choice

This Section presents a similar comparison to the previous section, this time to investigate the difference in results when the soil parameters are calculated from different soil texture data sets. Figure 11 shows the difference (WHS-IGBP) between diagnostics taken from the "corrected case" ensembles using the two soil texture datasets illustrated in Figure 1. The maps of changes in total column volumetric soil moisture (θ) and in β (Fig. 11a,b) have far more spatial variability than the equivalents from the previous comparison (Fig. 7a,b). The change of source data set alters all of the parameters calculated from Equations 9-14. Given the simple dependence of K_s, Ψ_s, θ_s and b on the fractions of sand and clay, there will be a high degree of correlation between the changes in any two of them. The changes in the latter three are all positively correlated with each other, which therefore produce a change in the same direction for θ_c and θ_w (Equations 13 and 14). The K_s change is negatively correlated with all the others. This is illustrated in Figures 12 and 13. Fig. 12a,b shows the absolute difference in θ_w and θ_c (c.f. Fig. 7c,d for the effect of the correction, noting the different colour scale),

---

[1] These numbers differ due to the averages being taken over different sets of grid cells: for each ensemble, Ω is only calculated where σ is large enough. This differs between ensembles, so the averages in Table 1 represent slightly different areas of the land surface, the intersection of which is shown in Figs. 7g, and 10.

and Fig. 12c,d show the absolute differences in θ_s and b (which were not affected by the correction). Figure 13 is equivalent to Figure 8, showing the ratios of K_s, θ_w, θ_c and $\theta_c - \theta_w$.
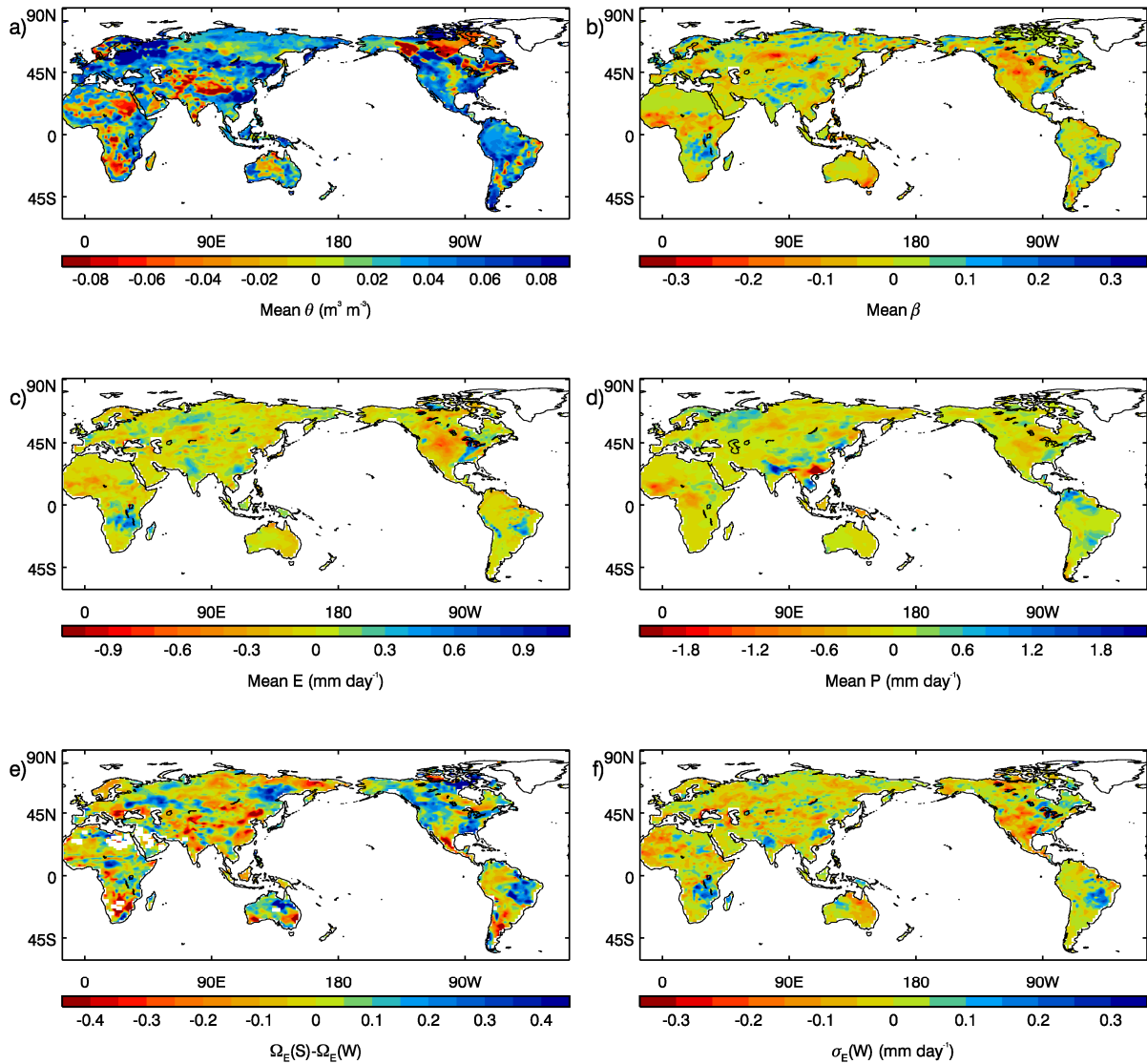
Figure 11: Difference maps (WHS–IGBP) for diagnostics from the "corrected case" experiments: a) mean total column soil moisture; b) mean soil moisture availability factor; c) mean evaporation; d) mean total precipitation; e) soil moisture-evaporation coupling; f) evaporation standard deviation. Means and standard deviations are based on six day averages from the W ensembles.

The patterns of all these changes are very similar to the pattern of sand fraction in the WHS data set (Figure 1 upper left). As discussed in Section 2.1, the WHS data has greater extremes of sand fraction than the IGBP data, which has a smoother pattern and narrower range of sand fractions (sandier soils over most of the globe but slightly less sand in areas which WHS designates as sandy). Hence the difference in sand fraction (WHS-IGBP) has a similar pattern to the WHS sand fraction. It is this aspect of the difference in the data sets that appears to dominate the difference in the parameters. Regions with a low proportion of sand in the WHS data set (and therefore a decrease relative to IGBP) show a decrease in K_s and an increase for all the other parameters, and vice versa. These changes may be expected to work consistently to produce an increase in volumetric soil moisture (Fig. 11a): the hydraulic conductivity, K, will decrease due to the reduction in K_s and the increase in both θ_s and b (Equation 7). This produces a moistening of the soil through slower drainage (Eq. 6), as discussed in Section 5. An increase in the saturation level (θ_s) may automatically increase the soil moisture in wet regions if the soil

is close to saturation. In vegetated regions, the increase in θ_w and $\theta_c - \theta_w$ may reduce β through Equation 4 (depending how large the existing change in soil moisture is, and whether the plants are moisture-stressed) and therefore reduce evaporation, feeding back into an additional increase in soil moisture. Given the high degree of correlation between these parameter changes, and their consistent effect on the soil moisture change, it would be difficult to establish their relative significance, which will vary spatially due to variations in soil type, vegetation cover and local meteorology. As expected, the change in soil moisture (Fig. 11a) has a very similar pattern to those of all the parameter changes.
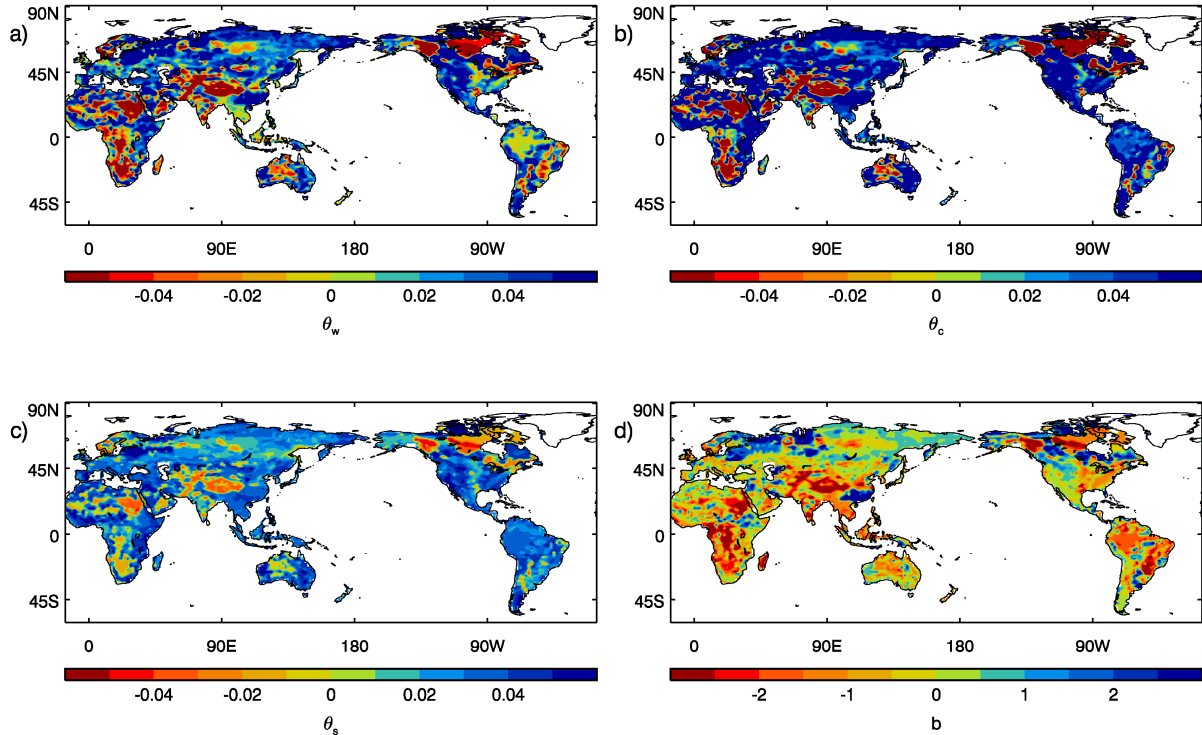
Figure 12: Difference maps (WHS-IGBP) for parameters used in the "corrected case" experiments: volumetric soil moisture at (a) wilting point, (b) critical point, (c) saturation; d) Clapp and Hornberger *b* parameter.

Over many regions of the world, the change in β (Fig. 11b) is consistent with the changes in θ_w and θ_c for vegetated regions, increasing in sandy areas (parts of east Africa, India and China), and decreasing elsewhere. In the northern hemisphere, in particularly wet regions of Europe, Russia, Canada and the eastern United States, the change in β is quite heterogeneous. Figure 5 (left) shows that β is close to one in these regions for both experiments, so the difference in β is likely to be caused by changes in how θ evolves relative to the altered critical point, θ_c. These patterns are roughly consistent with the pattern of sand fraction in the IGBP data (Fig. 1 upper right) which, given the relative uniformity of the WHS data in these regions, will dominate the difference pattern. In southern Africa and Brazil, we see the increase in β caused by slower soil drainage through the dry season which was also evident in analysing the effect of the correction (Section 5).

The change in evaporation (Figure 11c) is largely consistent with the change in β. The major exception seems to be in the sandy (according to WHS) region of China, where an increase in β does not translate into a discernable increase in evaporation. This is probably because the vegetation here is dominated by shrubs and C4 grasses (not shown), which have relatively small transpiration compared to other plant types. Overall, the difference is slightly negative (areal average −0.017 mm day^{-1}). Given the complex nature of the precipitation feedbacks (Section 3), and the heterogeneity of the land surface changes, it is unsurprising that the precipitation changes are different to the evaporation changes (Fig. 11c,d). On average, precipitation over land is increased by 0.009 mm day^{-1}.
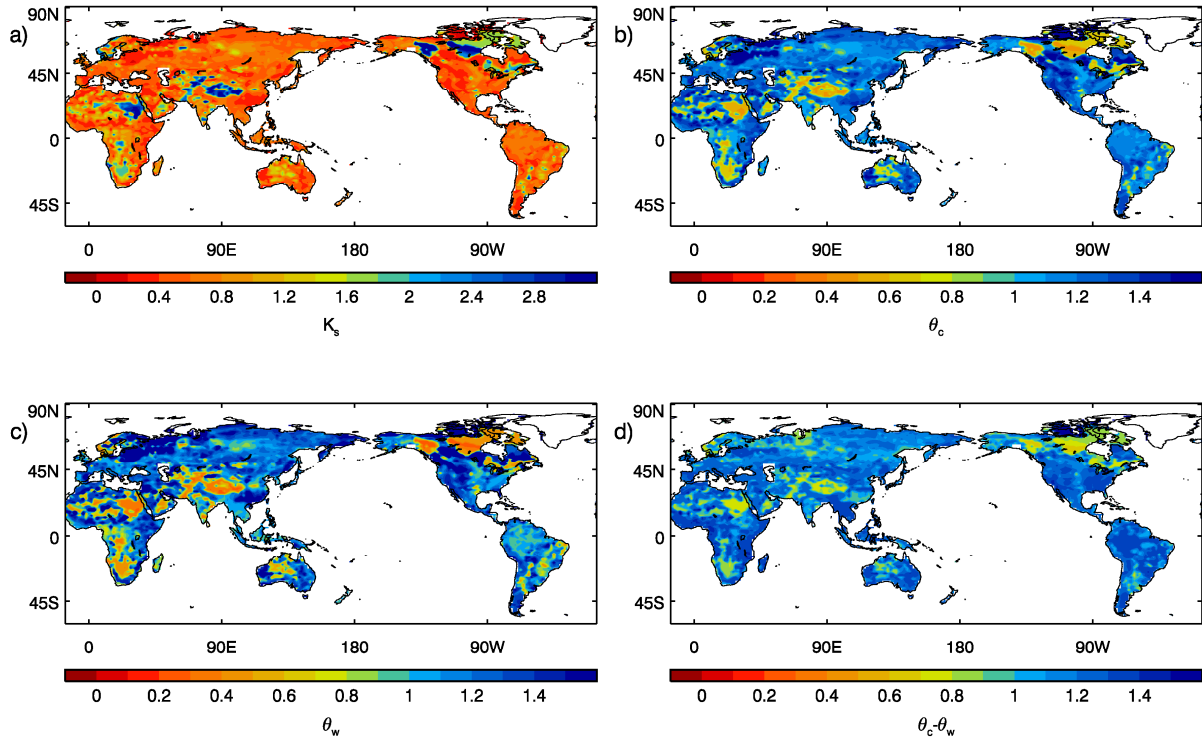
Figure 13: Ratio of WHS to IGBP soil parameters for corrected cases: a) hydraulic conductivity at saturation; volumetric soil moisture at (b) critical point and (c) wilting point and (d) their difference.

The difference in the soil moisture-evaporation coupling diagnostic ($\Omega_E(S) - \Omega_E(W)$, Fig. 11e) is not noticeably constrained by the difference in β. This is not surprising given the large spread of points in Figure 6 (left) and the relatively small differences in β displayed in Figure 11b compared to Figure 7b. It is curious that the increase in Eastern Brazil due to the algorithm correction (Fig. 7g) is also visible here, suggesting a consistent effect on the range of soil moisture in the W ensemble.

The annual cycle of precipitation and soil moisture in this region (not shown) is similar to that in the southern Africa region shown in Figure 9 for the WHS cases. Both the "uncorrected WHS" case, and the "corrected IGBP" case have larger downward moisture fluxes (higher K) than the "corrected WHS" case. The soil moisture in each ensemble member therefore approaches its minimum earlier in this dry season and so the proximity to this limit naturally reduces the spread between ensemble members.
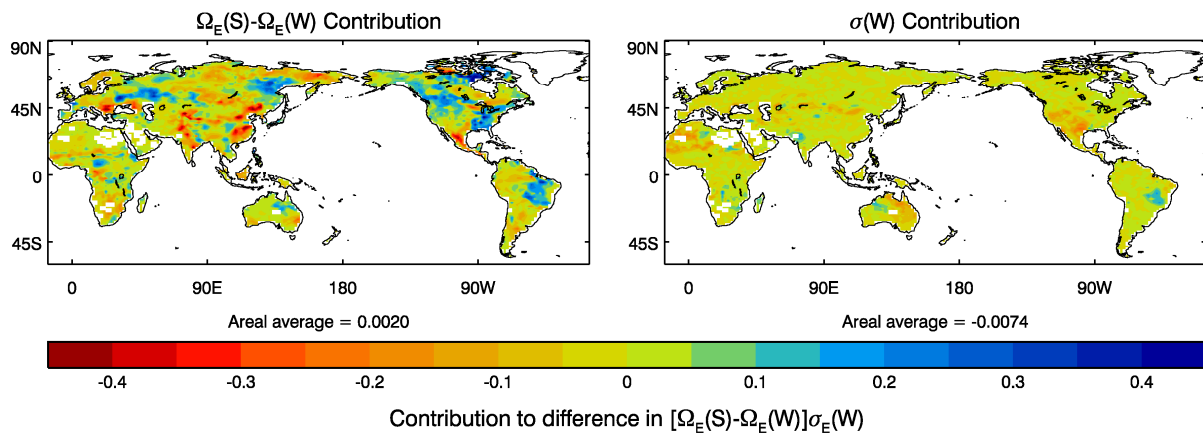
Figure 14: As Figure 10, but for difference in soil dataset (WHS-IGBP with corrected algorithm).

The difference in the variability of evaporation (Fig. 11f) is once again consistent with the difference in the means of soil moisture availability and evaporation (Fig. 11b and c) and is negative over most of

the globe. Figure 14 is equivalent to Figure 10, displaying the contributions of each factor to the difference in the overall coupling diagnostic $[\Omega_E(S) - \Omega_E(W)]\sigma_E(W)$. Locally, the contribution of the difference in $\Omega_E(S) - \Omega_E(W)$ is larger than that of $\sigma(W)$. However, since the sign of that difference is not consistent across the globe, it is the decrease in $\sigma(W)$ that once again dominates the global average, and is responsible for the overall decrease in land-atmosphere coupling noted in Section 3.

7 Discussion

The method of the Global Land-Atmosphere Coupling Experiment (GLACE; Koster et al., 2004, 2006) has been applied to a recent version of the Met Office Hadley Centre's atmospheric GCM, HadGEM3-A. The results show that HadGEM3-A has a strong precipitation response to soil moisture which was lacking in its predecessor HadAM3, particularly in the Sahel region of Africa, and to a lesser extent in the southern US. Consistent with the work of Guo et al. (2006) and Lawrence and Slingo (2005), this increase in coupling strength cannot be explained by developments in the land surface scheme. In addition to testing the response of the new atmosphere model, the effect on land-atmosphere coupling when different soil hydraulic parameters are used has also been investigated. The recent correction to the algorithm which generates these parameters (based on the equations of Cosby et al., 1984) provides an ideal test case: because the correction produces a near-uniform change in mean evaporation across the globe, we have a simple scenario to begin understanding the land surface's effects on land-atmosphere coupling. This simple case then helps to inform the slightly more complex changes which arise when the soil parameters are calculated from the soil texture datasets presented by Wilson and Henderson-Sellers (1985) or IGBP (Global Soil Data Task, 2000).

Following the approach of Guo et al. (2006), the path of the soil moisture's influence on precipitation was separated into two segments, investigating the soil moisture-evaporation coupling separately from the effect of evaporation on precipitation. Comparing the global averages for our four experiment cases, the soil moisture-evaporation segment of the coupling and the overall soil moisture-precipitation coupling are consistently ranked. Since the soil moisture-evaporation segment of the coupling is better constrained than the soil moisture-precipitation coupling, the analysis focused on this to understand the effects of altering soil parameters. Guo et al. (2006) identified two factors which contribute to this segment of the coupling: the strength of the soil moisture's control on evaporation and the variability of that evaporation. Both of these must be relatively high in order to feed into a soil moisture influence on the atmosphere.

The present work found that both of these factors are strongly affected by the soil moisture availability (which in the Unified Model is measured by the variable β). In geographical regions where moisture availability is very low (low β), such as the Sahara, evaporation is strongly constrained by this moisture availability, but evaporation variability is also low. So land-atmosphere coupling is weak in these regions. Conversely, where soil moisture is plentiful (high β), such as northern Europe, evaporation variability is high but the soil moisture influence on evaporation is low. So again land-atmosphere coupling is weak. Land-atmosphere coupling is therefore maximised in the semi-arid regions (Koster et al., 2004).

The choice of soil parameters affects β by two main mechanisms. First, by the hydraulic conductivity, K, which controls the vertical moisture fluxes through the soil. K is highest for coarse-textured (sandy) soils, which therefore drain and dry out more quickly than fine-textured (clay) soils (Equations 6-12). So fine textured soils tend to be moister on average than coarser ones. The two soil texture datasets tested differ most in their allocation of sand fraction, so K also differs between them. The correction to the algorithm increases the range of K, increasing it in sandy regions and decreasing it elsewhere. The second main mechanism by which the choice of soil parameters affect moisture availability is via the range of the stress interval: plants are moisture-stressed if the volumetric soil moisture lies below the critical point, θ_c and above the wilting point, θ_w. Both the choice of soil texture

data and the correction to the algorithm affect these parameters. The correction increased the level and range of this interval globally, so that moisture availability is decreased almost everywhere despite a widespread moistening of the soil due to decreased K. Similarly, the choice of soil texture dataset increases the range and level of the interval everywhere that K is decreased (and vice versa), so that a moistening of the soil due to the K change does not lead to an increase in moisture availability to plants for most regions. Southern hemisphere regions whose precipitation is controlled by the seasonal procession of the inter-tropical convergence zone are the main exception.

Since moisture availability is reduced nearly everywhere by the algorithm correction, we see an increase in soil moisture's control on evaporation, and a decrease in evaporation variability. The difference in β between the two soil texture datasets is smaller and the sign varies geographically, although the global average is slightly higher using the IGBP data, giving higher evaporation variability. For all the comparisons presented here, the effect on evaporation variability dominates the difference in the overall coupling diagnostics, but this is unlikely to be true universally: the GFS-OSU model used in the original GLACE intercomparison had low soil moisture influence on evaporation, but relatively high evaporation variability (Guo et al., 2006). Given that the significance of a change in each factor depends on the size of the other factor (Section 5), a change to the soil moisture-evaporation coupling strength would likely be dominant for that case.

It is desirable to understand how the developments from HadAM3 to HadGEM3-A have brought about the increase in coupling strength, but in practice it may prove impossible to isolate the improvement to any individual change. The interdependency of the new boundary layer and convection parametrizations with each other and with the enhanced vertical and horizontal resolution and new dynamical core make it difficult and somewhat artificial to design any interim model configurations that may be tested. Indeed, it is likely that the increased coupling is due to a combination of these developments and their interactions.

Having established the existence of an influence of soil moisture on precipitation within this new model, the investigation should turn to the nature of that influence. Further work will therefore use more detailed diagnostics from these experiments to understand the mechanisms by which soil moisture influences precipitation in HadGEM3-A, and whether these are consistent with those observed in the real world and other, more detailed, modelling studies (such as those mentioned in Section 3). Once understood, it may also be possible to compare diagnostics from HadAM3 to see which of these mechanisms were not present for the original GLACE model intercomparison.

Acknowledgements

References

Beljaars, A. C. M., Viterbo, P., Miller, M. J., and Betts, A. K. (1996). The anomolous rainfall over the united states during July 1993: Sensitivity to land surface parameterization and soil moisture anomalies. *Mon. Weather Rev.,* 124:362–383.

Clapp, R. B. and Hornberger, G. M. (1978). Empirical equations for some soil hydraulic properties. *Water Resour. Res.,* 14:601–604.

Compton, E. (2008). Comparing JULES soil hydraulic formulations over Fluxnet sites. Unpublished, Met Office.

Cosby, B. J., Hornberger, G. M., Clapp, R. B., and Ginn, T. R. (1984). A statistical exploration of the relationships of soil moisture characteristics to the physical properties of soils. *Water Resour. Res.,* 20:682–690.

Cox, P., Betts, R., Bunton, C., Essery, R., Rowntree, P., and Smith, J. (1999). The impact of new land surface physics on the GCM simulation of climate and climate sensitivity. *Clim. Dyn.,* 15:183–203.

Dharssi, I., Vidale, P., Verhoef, A., Macpherson, B., Jones, C., and Best, M. (2009). New soil physical properties implemented in the Unified Model at PS18. Met Office Tech Note 528, Met Office.

Essery, R., Best, M., and Cox, P. (2001). MOSES 2.2 technical documentation. Hadley Centre Technical Note 30, Hadley Centre, Met Office, Fitzroy Road, Exeter, UK.

Findell, K. and Eltahir, E. (2003). Atmospheric controls on soil moisture-boundary layer interactions. Part I: Framework development. *J. Hydromet.,* 4(3):552–569.

Gates, W. L., Boyle, J. S., Covey, C., Dease, C. G., Doutriaux, C. M., Drach, R. S., Fiorino, M., Gleckler, P. J., Hnilo, J. J., Marlais, S. M., Phillips, T. J., Potter, G. L., Santer, B. D., Sperber, K. R., Taylor, K. E., and Williams, D. N. (1999). An overview of the results of the Atmospheric Model Intercomparison Project (AMIP I). *Bull. Am. Meteorol. Soc.,* 80(1):29–55.

Global Soil Data Task (2000). Global soil data products CD-ROM (IGBP-DIS). CD-ROM. International Geosphere-Biosphere Programme, Data and Information System, Potsdam, Germany. Available from Oak Ridge National Laboratory Distributed Active Archive Center, Oak Ridge, Tennessee, U.S.A.

Guo, Z., Dirmeyer, P. A., Koster, R. D., Bonan, G., Chan, E., Cox, P., Gordon, C. T., Kanae, S., Kowalczyk, E., Lawrence, D., Liu, P., Lu, C.-H., Malyshev, S., McAvaney, B., McGregor, J. L., Mitchell, K., Mocko, D., Oki, T., Oleson, K. W., Pitman, A., Sud, Y. C., Taylor, C. M., Verseghy, D., Vasic, R., Xue, Y., and Yamada, T. (2006). GLACE: The Global Land-Atmosphere Coupling Experiment. Part II: Analysis. *J. Hydromet.,* 7(4):611–625.

Hewitt, H. T., Copsey, D., Culverwell, I. D., Harris, C. M., Hill, R. S. R., Keen, A. B., McLaren, A. J., and Hunke, E. C. (2011). Design and implementation of the infrastructure of HadGEM3: the next-generation Met Office climate modelling system. *Geoscientific Model Development*, 4(2):223–253, doi:10.5194/gmd-4-223-2011.

Hohenegger, C., Brockhaus, P., Bretherton, C. S., and Schaer, C. (2009). The soil moisture-precipitation feedback in simulations with explicit and parameterized convection. *J. Climate,* 22(19):5003–5020, doi:10.1175/2009JCLI2604.1.

Johansen, O. (1975). Thermal conductivity of soils. PhD thesis, University of Trondheim, Norway.

Koster, R., Dirmeyer, P., Guo, Z., Bonan, G., Chan, E., Cox, P., Gordon, C., Kanae, S., Kowalczyk, E., Lawrence, D., Liu, P., Lu, C.-H., Malyshev, S., McAvaney, B., Mitchell, K., Mocko, D., Oki, T., Oleson, K., Pitman, A., Sud, Y., Taylor, C., Verseghy, D., Vasic, R., Xue, Y., and Yamada, T. (2004). Regions of strong coupling between soil moisture and precipitation. *Science,* 305:1137–1140.

Koster, R. D., Guo, Z., Dirmeyer, P. A., Bonan, G., Chan, E., Cox, P., Davies, H., Gordon, C. T., Kanae, S., Kowalczyk, E., Lawrence, D., Liu, P., Lu, C.-H., Malyshev, S., McAvaney, B., Mitchell, K., Mocko, D., Oki, T., Oleson, K. W., Pitman, A., Sud, Y. C., Taylor, C. M., Verseghy, D., Vasic, R., Xue, Y., and Yamada, T. (2006). GLACE: The Global Land-Atmosphere Coupling Experiment. Part I: Overview. *J. Hydromet.,* 7(4):590–610.

Koster, R. D., Guo, Z., Yang, R., Dirmeyer, P. A., Mitchell, K., and Puma, M. J. (2009). On the nature of soil moisture in land surface models. *J. Climate,* 22(16):4322–4335, doi:10.1175/2009JCLI2832.1.

Koster, R. D., Mahanama, S. P. P., Yamada, T. J., Balsamo, G., Berg, A. A., Boisserie, M., Dirmeyer, P. A., Doblas-Reyes, F. J., Drewitt, G., Gordon, C. T., Guo, Z., Jeong, J.-H., Lawrence, D. M., Lee, W.-S., Li, Z., Luo, L., Malyshev, S., Merryfield, W. J., Seneviratne, S. I., Stanelle, T., van den Hurk, B. J. J. M., Vitart, F., and Wood, E. F. (2010). Contribution of land surface initialization to subseasonal forecast skill: First results from a multi-model experiment. *Geophys. Res. Lett.*, 37, doi:10.1029/2009GL041677.

Lawrence, D. and Slingo, J. (2005). Weak land-atmosphere coupling strength in HadAM3: The role of soil moisture variability. *J. Hydromet.,* 6(5):670–680.

Mercado, L., Huntingford, C., Gash, J., Cox, P. M., and Jogireddy, V. (2007). Improving the representation of radiation interception and photosynthesis for climate model applications. *Tellus B,* 59:553–569, doi:10.1111/j.1600-0889.2007.00256.x.

Moufouma-Okia, W. and Rowell, D. P. (2010). Impact of soil moisture initialisation and lateral boundary conditions on regional climate model simulations of the West African Monsoon. *Clim. Dyn.,* 35:213–229, doi:10.1007/s00382-009-0638-0.

Seneviratne, S. I., Corti, T., Davin, E. L., Hirschi, M., Jaeger, E. B., Lehner, I., Orlowsky, B., and Teuling, A. J. (2010). Investigating soil moisture-climate interactions in a changing climate: A review. *Earth-Science Reviews,* 99(3-4):125 – 161, doi:10.1016/j.earscirev.2010.02.004.

Senior, C., Arrabas, A., Brown, A. R., Cullen, M., Johns, T., Martin, G., Milton, S., Webster, S., and Williams, K. (2011). *The development of atmospheric general circulation models: complexity, synthesis and computation*, chapter 5, pages 86–89. Cambridge University Press.

Taylor, C. M. (2008). Intraseasonal Land-Atmosphere Coupling in the West African Monsoon. *J. Climate,* 21(24):6636–6648, doi:10.1175/2008JCLI2475.1.

Walters, D. N., Best, M. J., Bushell, A. C., Copsey, D., Edwards, J. M., Falloon, P. D., Harris, C. M., Lock, A. P., Manners, J. C., Morcrette, C. J., Roberts, M. J., Stratton, R. A., Webster, S., Wilkinson, J. M., Willett, M. R., Boutle, I. A., Earnshaw, P. D., Hill, P. G., MacLachlan, C., Martin, G. M., Moufouma-Okia, W., Palmer, M. D., Petch, J. C., Rooney, G. G., Scaife, A. A., and Williams, K. D. (2011). The Met Office Unified Model Global Atmosphere 3.0/3.1 and JULES Global Land 3.0/3.1 configurations. Geoscientific Model Development Discussions, 4(2):1213–1271, doi:10.5194/gmdd-4-1213-2011.

Wei, J. and Dirmeyer, P. A. (2010). Toward understanding the large-scale land-atmosphere coupling in the models: Roles of different processes. *Geophys. Res. Lett.,* 37, doi:10.1029/2010GL044769.

Wilson, M. F. and Henderson-Sellers, A. (1985). A global archive of land cover and soils data for use in general circulation climate models. *J. Climatol.,* 5:119–143.

Zhang, L., Dirmeyer, P. A., Wei, J., Guo, Z., and Lu, C.-H. (2011). Land-Atmosphere Coupling Strength in the Global Forecast System. *J. Hydromet.,* 12(1):147–156, doi:10.1175/2010.JHM1319.1.